Journal of Sound and Vibration (2002) **249**(4), 785–813
doi:10.1006/jsvi.2001.3912, available online at http://www.idealibrary.com on IDEAL®

A COMPARISON OF THREE TECHNIQUES USING STEADY STATE DATA TO IDENTIFY NON-LINEAR MODAL BEHAVIOR OF AN EXTERNALLY EXCITED CANTILEVER BEAM

T. A. Doughty, P. Davies and A. K. Bajaj

Ray W. Herrick Laboratories, School of Mechanical Engineering, Purdue University, W. Lafayette, IN 47907-1077, *U.S.A.*

(*Received* 28 *August* 2000, *and in final form* 16 *July* 2001)

Non-linear system identification is used to generate models of modes in physical structures. Analysis of the theoretical non-linear model of a cantilevered beam is used to predict the inputs to the physical system that will produce responses suitable for enhanced parameter estimation, thereby improving the model. Three identification techniques are described and applied to both numerical and experimental data: the first is based on the continuous-time differential equation model of the system, the second uses relationships generated by the method of harmonic balance, and the third is based on fitting steady state response data to the amplitude and phase modulation equations resulting from a multiple time scales analysis. The performance of each method improves as the non-linearities in the system become more pronounced. The benefits and limitations of the methods are discussed.

1. INTRODUCTION

Non-linear systems display a wide variety of interesting behavior, from jumps in the response to amplitude-modulated motions and chaos. The conditions under which the system exhibits a particular behavior depends on the system parameters, the initial conditions and the nature of the excitation. Small changes in any of these may lead to very different response characteristics. Seeking out this interesting behavior in an experimental system may be nearly impossible without analysis of accurate models of the system to guide the experimenter, hence the need for system identification to develop accurate models of the system.

System identification [1–5] is an iterative process, each iteration consisting of three major components: model structure identification, model parameter estimation, and model evaluation. These components are not three distinct procedures: they are intertwined because a model structure cannot be fully evaluated without knowing the model parameters and determining how close the observed and predicted responses are. Broadly speaking, there are three approaches to non-linear system identification: physical model based; non-parametric involving higher order spectra and Volterra kernal estimation; and hybrid methods based on very general non-linear models. The last approach include regression models with terms that are polynomial combinations of the states (displacement, velocity, etc.), models with terms that are polynomial combinations of measurement samples, or artificial neural network models. The third approach usually requires the use of model order and term selection algorithms to prune the models [6–10]. In practice, all approaches

0022-460X/02/040785 + 29 $35.00/0

require *a priori* knowledge of the system in order to make the identification computationally manageable. This knowledge may come directly from the physics of the system or from observations and analysis of measurements of the system behavior.

While theory can occasionally be used to construct complete models of vibrating systems, it is rare that these models fully predict the behavior of their physical counterparts. While qualitative agreement between the theory and experiment is often achieved, indicating some success with model structure identification, quantitative agreement is more difficult [11–14], especially with more complex systems such as those with internal resonances [15–17]. Imperfections in materials, non-ideal boundary conditions, and assumptions made in the development of the analytical model, are typically the major causes of the experiment–theory mismatch [18, 17]. As the validity of the assumptions deteriorates, the gap between the physical system and the mathematical model behavior tends to grow. This gap prompts a re-evaluation of assumptions, such as described in the work of Zaretzky and Crespo da Silva [19], usually aided by observations of system responses under various excitation conditions. This, in turn, leads to a restructuring of the theoretical model; this is all part of the system identification process.

Even when the model structure is correct, estimates of the parameters associated with specific terms in the model will be poor if the response data used in the estimation is not strongly dependent on the presence of those terms. The experimentalist, therefore, must create excitation conditions to reveal the non-linearities (e.g., see references [11, 12]). The problem is in determining the desirable excitation conditions. This is where analysis of the theoretical model of the system plays an important role. Theoretical analysis based on approximations to the model coefficients could be used to determine regions where significant non-linear responses are most likely to occur. Experimentally exploring these regions, and comparing model predictions to measured response characteristics can help identify the excitations that result in the most useful data for system identification.

The focus of this paper is on the evaluation of the performance of three parameter estimation techniques when used to estimate the parameters of a model of the response of one mode of a base excited cantilever beam undergoing transverse vibrations. The three techniques are based on a continuous-time differential equation model of the system. One technique utilizes the differential equation directly and the other two techniques are based on approximations of the steady state response to harmonic excitation. The methods are tested with steady state harmonic response data, because two of the methods are restricted to this form of excitation. The approach is applied to a theoretical model for the beam responding in its second mode of vibration. Extensive simulations were carried out to determine the excitation conditions that would lead to accurate model parameter estimates, and to determine the effect of the measurement procedure (filtering, quantization, and sampling) on the parameter estimation. The interplay of simulation and experiment is used throughout the identification procedure to help gain an understanding of the causes of problems associated with accurate parameter estimation.

2. THEORETICAL INVESTIGATION

2.1. SINGLE MODE RESPONSE OF A CANTILEVER BEAM

A schematic of a horizontally mounted cantilevered beam subject to vertical excitation of the clamped base is shown in Figure 1. If in-plane motions only are considered, the equations of motion developed in references [17, 20] reduce to the following integro-differential equation:

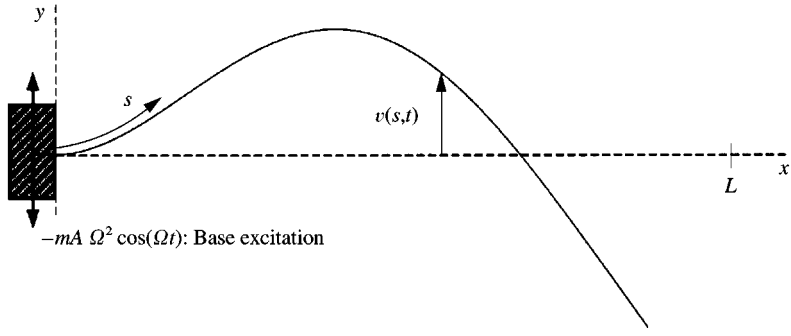

Figure 1. Theoretical configuration for the base excited cantilever beam. System variables are: m, mass per unit length; c, damping per unit length; D_ξ, bending stiffness; A, amplitude of base displacement; Ω, forcing frequency; s, reference variable; L, beam length.

$$m\ddot{v} + c\dot{v} + D_\xi\{v^{iv} + [v'(v'v'')']'\} = -mA\Omega^2\cos(\Omega t)$$

$$-\frac{m}{2}\left\{v'\int_L^s\int_0^\zeta (v'^2\,\mathrm{d}\eta)^{\cdot\cdot}\mathrm{d}\zeta\right\}', \tag{1}$$

$$v(0,t) = v'(0,t) = v''(L,t) = v'''(L,t) = 0, \tag{2}$$

where "$\cdot$" refers to derivative with respect to time, and "$'$" refers to derivative with respect to the spatial co-ordinate s. The non-linear term on the left-hand side of the equation is due to the curvature of the beam, and the one on the right-hand side is the result of inertial effects. The non-linear terms that need to be included in the theoretical model are based on the system's geometry, boundary conditions, and form of excitation. To make the analysis more general, equation (2) is non-dimensionalized by applying the following scalings:

$$s^* = \frac{s}{L}, \quad v^* = \frac{v}{L}, \quad c^* = c\left[\frac{L^4}{mD_\xi}\right]^{1/2},$$
$$t^* = t\left[\frac{D_\xi}{(mL^4)}\right]^{1/2}, \quad A^* = A\frac{L^3}{D_\xi}, \quad \Omega^* = \Omega\left[\frac{mL^4}{D_\xi}\right]^{1/2}, \tag{3}$$

which results in

$$\ddot{v} + c\dot{v} + v^{iv} = -A\Omega^2\cos(\Omega t) - \{v'(v'v'')'\}'$$

$$-\frac{1}{2}\left\{v'\int_1^s\int_0^\zeta (v'^2\,\mathrm{d}\eta)^{\cdot\cdot}\mathrm{d}\zeta\right\}', \tag{4}$$

$$v(0,t) = v'(0,t) = v''(1,t) = v'''(1,t) = 0. \tag{5}$$

For simplicity, the "*" notation associated with dimensionless parameters and variables is dropped, and in the rest of the development all the parameters are dimensionless.

Next, it is assumed that the response is dominated by one mode of vibration, the spatial dependence being in the form of the linear mode shape, $\phi(s)$. Hence, the response is written as

$$v(s,t) = a(t)\phi(s), \tag{6}$$

where $\phi(s)$ is obtained by solving, with appropriate boundary conditions (equations (5)), equation (4) with the forcing, damping and non-linear terms set to zero. This results in

$$\phi(s) = C[\sin(\beta s) - \sinh(\beta s) - \alpha(\cos(\beta s) - \cosh(\beta s))], \tag{7}$$

where

$$\alpha = \frac{\sin(\beta) + \sinh(\beta)}{\cos(\beta) + \cosh(\beta)}$$

and where the amplitude C of the modal function has been chosen so that $\int_0^1 \phi^2 \, ds = 1$. For the second mode of the beam, the mode studied in the experiments described later, the constant $\beta = 4{\cdot}694091$.

Substituting equation (6) into equation (4), multiplying the resulting expression by $\phi(s)$, and integrating over the length of the beam results in the temporal equation

$$\ddot{a} + c\dot{a} + \omega_0^2 a = \alpha_0(-A\Omega^2)\cos(\Omega t) - \alpha_1 a^3 - \alpha_2(a\dot{a}^2 + a^2\ddot{a}). \tag{8}$$

In this equation, the natural frequency is defined by $\omega_0 = \beta^2$, the contribution of the non-linear curvature term is

$$\alpha_1 = \int_0^1 (\phi\phi''^3 + 4\phi\phi'\phi''\phi''' + \phi\phi'^2\phi^{iv}) \, ds, \tag{9}$$

the contribution of the non-linear inertial term is

$$\alpha_2 = \int_0^1 \left\{ \phi' \int_1^s \int_0^\zeta \phi'^2 \, d\eta \, d\zeta \right\}' \phi \, ds \tag{10}$$

and the scaling coefficient associated with the forcing term is

$$\alpha_0 = \int_0^1 \phi \, ds. \tag{11}$$

Having determined the one-mode model for the base excited cantilever beam, the goal of the research is to evaluate the various model parameter estimation techniques by estimating the various linear and non-linear coefficients in equation (4). The theoretical definitions of these parameters in equations (9)–(11) will serve as one check on these techniques.

2.2. SYSTEM IDENTIFICATION METHODS

2.2.1. *Continuous-time system identification*

In this identification approach, measured or derived states at various times (e.g., displacement, velocity and acceleration) are used with the differential equation model of the system to set up a matrix equation [5] to solve for the model parameters.

In the investigation, ω_0 was measured experimentally and, therefore, is treated here as a known parameter. Thus, equation (8) is re-written in vector form as

$$(\ddot{a} + \omega_0^2 a) = [-\dot{a}, F(t), -a^3, -(a\dot{a}^2 + a^2\ddot{a})][c, \alpha_0, \alpha_1, \alpha_2]^T, \tag{12}$$

where $F(t) = (-A\Omega^2)\cos(\Omega t)$. The elements of the vector $\mathbf{P} = [c, \alpha_0, \alpha_1, \alpha_2]^{\mathrm{T}}$ are referred to as the model parameters which are the unknowns. The system's input $F(t)$ and response $a(t)$ are measured and, by using the data at sample times, (t_i), $i = 1, 2, 3, \ldots, N$, a known vector $\mathbf{K}$ and a matrix $\mathbf{A}$ are generated. Here, $\mathbf{K} = [\ddot{a}(t_1) + \omega_0^2 a(t_1),\ \ddot{a}(t_2) + \omega_0^2 a(t_2),\ \ddot{a}(t_3) + \omega_0^2 a(t_3), \ldots, \ddot{a}(t_N) + \omega_0^2 a(t_N),]^{\mathrm{T}}$, and a row of the matrix $\mathbf{A}$ are the elements of the row vector on the right-hand side of equation (12) evaluated at a particular sample time. Thus, for example, the first column of $\mathbf{A}$ is $[-\dot{a}(t_1),\ -\dot{a}(t_2),\ -\dot{a}(t_3), \ldots, -\dot{a}(t_N)]^{\mathrm{T}}$. Now assuming that the model parameters do not change with time, the parameter vector $\mathbf{P}$ may be estimated by solving (in a least-squares sense) the matrix equation

$$\mathbf{K} = \mathbf{A} \cdot \mathbf{P}. \tag{13}$$

Typically for a one-mode model, only one of the states is measured in an experiment, and the other states are calculated from this state by using numerical differentiation or integration schemes [21]. This procedure tends to amplify, respectively, high- or low-frequency noise, in the measurements. In the experiments described later, acceleration measurements were integrated 2 times to produce estimates of velocity and displacement. High levels of low-frequency noise resulting from the integrations can be reduced by high-pass filtering the state signals prior to forming the matrices $\mathbf{A}$ and $\mathbf{K}$.

To avoid aliasing during the measurement process, signals are passed through low-pass anti-aliasing filters prior to sampling. Even if the excitation is at a single frequency, the response of a non-linear system will contain higher harmonics, and the anti-aliasing filter will remove some of these harmonics. To ensure that information at frequencies associated with significant harmonics is not removed, sampling rates, and thus anti-aliasing cut-off frequencies, may have to be set at very high levels. High sample rates may also lead to ill-conditioning of the set of equations used in the parameter estimation, which in turn can lead to large parameter estimation errors.

The displacement measurements $a(t)$ are bandlimited due to the anti-aliasing filter, and high frequencies are further attenuated in numerical integration. However, when the non-linear functions of states are calculated to form the columns of $\mathbf{A}$, they will contain higher frequencies. For example, $a^3(t)$, can contain frequencies up to 3 times the highest frequency in $a(t)$. Sample rates chosen in the original data acquisition may now be too low to satisfy the Nyquist criterion for signals such as $a^3(t)$. Thus, the order of the non-linearities must be taken into account when choosing an appropriate sample rate, so that no aliasing occurs when the signals that are non-linear functions of states are calculated.

The use of anti-aliasing filters causes errors by removing high-frequency content, and these errors propagate in the calculation of signals that are non-linear functions of states. These calculated signals, the columns of $\mathbf{A}$, will have high-frequency content that has been removed from the signal in the vector $\mathbf{K}$, which is a linear function of the acceleration and displacement. To reduce this mismatch of high-frequency information, the vector $\mathbf{K}$, and the signals that form the columns of $\mathbf{A}$, can be digitally filtered with a low-pass filter having a cut-off frequency set at, or below, the analog anti-aliasing filter cut-off frequency. A simple analysis that consists of splitting a into a low- and high-frequency part and low-pass filtering the terms of equation (8), can be shown to demonstrate that this does not completely alleviate the problem, because of combinations of quadratic high-frequency components multiplied by linear low-frequency components. However, if the high-frequency components removed by the anti-aliasing filters are small compared to the low-frequency components, the resulting terms in the filtered equations will be reasonably accurate.

2.2.2. *Harmonic balance based identification*

In the harmonic balance method [22], the system's output is assumed to be a truncated Fourier series whose fundamental frequency is related to the driving frequency. The Fourier truncated series is then substituted into the differential equation and terms of the same frequency are equated, resulting in a set of relationships between the spectral amplitudes of the excitation and those of the response. These relationships are functions of the unknown parameters in the differential equation.

Assume that the excitation and the response are of the form

$$F(t) = F_0 + F_{1c}\cos(\Omega t) + F_{1s}\sin(\Omega t) + F_{3c}\cos(3\Omega t) + F_{3s}\sin(3\Omega t),$$

$$a(t) = a_0 + a_{1c}\cos(\Omega t) + a_{1s}\sin(\Omega t) + a_{3c}\cos(3\Omega t) + a_{3s}\sin(3\Omega t).$$

Then substituting these expressions into equation (8) and equating the appropriate terms yields the matrix equation

$$\mathbf{F} = \mathbf{A}\cdot\mathbf{P}, \tag{14}$$

where $\mathbf{F} = [F_0, F_{1c}, F_{1s}, F_{3c}, F_{3s}]^{\mathrm{T}}$, $\mathbf{P} = [1/\alpha_0, c/\alpha_0, \omega_0^2/\alpha_0, \alpha_1/\alpha_0, \alpha_2/\alpha_0]^{\mathrm{T}}$,

$$\mathbf{A} = \begin{bmatrix} 0 & 0 & a_0 & c_0 & n_0 \\ -\Omega^2 a_{1c} & \Omega a_{1s} & a_{1c} & c_{1c} & n_{1c} \\ -\Omega^2 a_{1s} & -\Omega a_{1c} & a_{1s} & c_{1s} & n_{1s} \\ -9\Omega^2 a_{3c} & 3\Omega a_{3s} & a_{3c} & c_{3c} & n_{3c} \\ -9\Omega^2 a_{3s} & -3\Omega a_{3c} & a_{3s} & c_{3s} & n_{3s} \end{bmatrix}$$

and

$$\begin{aligned}
c_0 &= a_0^3 + \tfrac{3}{2}a_0a_{1c}^2 + \tfrac{3}{2}a_0a_{1s}^2 + \tfrac{3}{2}a_0a_{3c}^2 + \tfrac{3}{2}a_0a_{3s}^2,\\
c_{1c} &= 3a_0^2a_{1c} + \tfrac{3}{4}a_{1c}^3 + \tfrac{3}{4}a_{1c}a_{1s}^2 + \tfrac{3}{4}a_{1c}^2a_{3c} - \tfrac{3}{4}a_{1s}^2a_{3c} + \tfrac{3}{2}a_{1c}a_{3c}^2\\
&\quad + \tfrac{3}{2}a_{1c}a_{3s}^2 + \tfrac{3}{2}a_{1c}a_{1s}a_{3s},\\
c_{1s} &= 3a_0^2a_{1s} + \tfrac{3}{4}a_{1s}^3 + \tfrac{3}{4}a_{1c}^2a_{1s} + \tfrac{3}{4}a_{1c}^2a_{3s} - \tfrac{3}{4}a_{1s}^2a_{3s} + \tfrac{3}{2}a_{1s}a_{3c}^2\\
&\quad + \tfrac{3}{2}a_{1s}a_{3s}^2 - \tfrac{3}{2}a_{1c}a_{1s}a_{3c},\\
c_{3c} &= 3a_0^2a_{3c} + \tfrac{1}{4}a_{1c}^3 + \tfrac{3}{2}a_{1c}^2a_{3c} - \tfrac{3}{4}a_{1c}a_{1s}^2 + \tfrac{3}{2}a_{1s}^2a_{3c} + \tfrac{3}{4}a_{3c}^3 + \tfrac{3}{4}a_{3c}a_{3s}^2,\\
c_{3s} &= 3a_0^2a_{3s} - \tfrac{1}{4}a_{1s}^3 + \tfrac{3}{2}a_{1c}^2a_{3s} + \tfrac{3}{4}a_{1c}^2a_{1s} + \tfrac{3}{2}a_{1s}^2a_{3s} + \tfrac{3}{4}a_{3s}^3 + \tfrac{3}{4}a_{3c}^2a_{3s},\\
n_0 &= \Omega^2(-\tfrac{1}{2}a_0a_{1c}^2 - \tfrac{1}{2}a_0a_{1s}^2 - \tfrac{9}{2}a_0a_{3c}^2 - \tfrac{9}{2}a_0a_{3s}^2),\\
n_{1c} &= \Omega^2(-a_0^2a_{1c} - \tfrac{1}{2}a_{1c}^3 - \tfrac{1}{2}a_{1c}a_{1s}^2 - \tfrac{3}{2}a_{1c}^2a_{3c} + \tfrac{3}{2}a_{1s}^2a_{3c} - 3a_{1c}a_{1s}a_{3s}\\
&\quad - 5a_{1c}a_{3c}^2 - 5a_{1c}a_{3s}^2),
\end{aligned} \tag{15}$$

$$n_{1s} = \Omega^2(-a_0^2 a_{1s} - \tfrac{1}{2}a_{1s}^3 - \tfrac{1}{2}a_{1c}^2 a_{1s} - \tfrac{3}{2}a_{1c}^2 a_{3s} + \tfrac{3}{2}a_{1s}^2 a_{3s} + 3a_{1c}a_{1s}a_{3c} - 5a_{1s}a_{3c}^2 - 5a_{1s}a_{3s}^2),$$

$$n_{3c} = \Omega^2(-9a_0^2 a_{3c} - \tfrac{1}{2}a_{1c}^3 - 5a_{1c}^2 a_{3c} + \tfrac{3}{2}a_{1c}a_{1s}^2 - 5a_{1s}^2 a_{3c} - \tfrac{9}{2}a_{3c}^3 - \tfrac{9}{2}a_{3c}a_{3s}^2),$$

$$n_{3s} = \Omega^2(-9a_0^2 a_{3s} + \tfrac{1}{2}a_{1s}^3 - 5a_{1c}^2 a_{3s} - \tfrac{3}{2}a_{1c}^2 a_{1s} - 5a_{1s}^2 a_{3s} - \tfrac{9}{2}a_{3s}^3 - \tfrac{9}{2}a_{3c}^2 a_{3s}).$$

Rows 1–5 of equation (14) arise from equating the DC terms, the cos (Ωt) terms, the sin (Ωt) terms, the cos ($3\Omega t$) terms, and the sin ($3\Omega t$) terms respectively. The spectral amplitudes of the excitation ($F_0, F_{1c}, F_{1s}, F_{3c}, F_{3s}$), and response ($a_0, a_{1c}, a_{1s}, a_{3c}, a_{3s}$), are used to calculate the terms in **F** and **A**. By collecting steady state response data over a range of excitation frequencies (Ω), functions **F** and **A** in equation (14) may be augmented, each excitation frequency resulting in a set of five new equations. This augmented matrix equation may be used to determine least-squares estimates of the model parameters, **P**.

In this particular example, because of the cubic form of the non-linearities, if F_0 is zero then a_0 will also be zero. By setting F_0 and a_0 to zero, and treating ω_0 as a known parameter, equation (14) may be rewritten as

$$\mathbf{K} = \mathbf{A} \cdot \mathbf{P}, \tag{16}$$

where $\mathbf{K} = [\Omega^2 a_{1c} - \omega_0^2 a_{1c}, \Omega^2 a_{1s} - \omega_0^2 a_{1s}, 9\Omega^2 a_{3c} - \omega_0^2 a_{3c}, 9\Omega^2 a_{3s} - \omega_0^2 a_{3s}]^{\mathrm{T}}$, $\mathbf{P} = [c, \alpha_0, \alpha_1, \alpha_2]^{\mathrm{T}}$, and

$$\mathbf{A} = \begin{bmatrix} +\Omega a_{1s} & -F_{1c} & c_{1c} & n_{1c} \\ -\Omega a_{1c} & -F_{1s} & c_{1s} & n_{1s} \\ +3\Omega a_{3s} & -F_{3c} & c_{3c} & n_{3c} \\ -3\Omega a_{3c} & -F_{3s} & c_{3s} & n_{3s} \end{bmatrix}.$$

The terms in the third and fourth columns of **A** are as defined in equations (15), with a_0 set to zero.

A larger number of terms may be assumed in the Fourier series, and the same approach adopted, resulting in an expanded set of equations that are dependent on F_{ic}, F_{is}, a_{ic} and a_{is}, where the subscript i denotes the order of the term in the Fourier series. In principle, using a higher number of terms in the Fourier series leads to a more accurate approximation to the solution. However, in a system identification procedure, measured harmonic response amplitudes are used to estimate the system parameters. If the higher harmonics' amplitudes are small and sensitive to measurement noise, their inclusion will result in noisy terms in **F** and **A**, and this will adversely affect the estimation of **P**. Thus, a trade-off must be made between a better approximation and the introduction of noisy terms in the estimation.

The amplitudes of the harmonic components of $a(t)$ are estimated by first bandpass filtering the acceleration signal to remove low- and high-frequency noise; then modelling the filtered acceleration signal as a sum of harmonically related sine and cosine waves of known frequencies and fitting the model to the filtered data; and finally twice integrating, analytically, the terms in this estimated acceleration model. This was done in preference to using fast Fourier transforms to determine spectral amplitudes, a method that suffers from

spectral leakage due to windowing effects. The estimation of the spectral amplitudes is described in greater detail in the next section. It is convenient to use accelerometers to measure the beam's response, but in doing so the DC information in the displacement is lost. In the present application this does not cause any problem because if F_0 is zero, then a_0 is also zero. For other systems, e.g., those with quadratic non-linearities, this will not be the case and thus a_0 must be determined through an addition measurement, or by directly measuring displacement instead of acceleration.

2.2.3. *Multiple time scales based identification*

The third method of system identification utilizes the amplitude modulation equations which result from a multiple time scales analysis [23] of the system. Prior to performing this multiple time scales analysis, it is necessary to arrange the governing equation so that the damping, forcing, and non-linearities are of the same order. A small parameter ε is introduced, where $0 < \varepsilon \ll 1$. Now, rescaling the parameters by

$$a = \sqrt{\varepsilon} b, \quad \alpha_0(-A\Omega^2) = \varepsilon\sqrt{\varepsilon} 2\hat{k}, \quad c = \varepsilon\hat{c}, \tag{17}$$

equation (8) becomes

$$\ddot{b} + \Omega^2 b = \varepsilon 2\hat{k}\cos(\Omega t) - \varepsilon\alpha_1 b^3 - \varepsilon\alpha_2(b\dot{b}^2 - b^2\ddot{b}) - \varepsilon\hat{c}\dot{b} + \varepsilon\sigma b, \tag{18}$$

where the detuning, σ, is introduced with

$$\Omega^2 = \omega_0^2 + \varepsilon\sigma. \tag{19}$$

Note that in this formulation, the forcing amplitude $\hat{k}$ and the detuning frequency may be allowed to vary with time. While this freedom is not utilized in this study, both the continuous-time and the multiple time scales based identification methods may be applied in a non-stationary investigation. Exploration of the advantages of non-stationary excitation on parameter identification is the subject of ongoing research.

In the method of multiple time scales, time-like independent quantities are introduced such that

$$T_0 = t, \quad T_1 = \varepsilon t, \quad T_2 = \varepsilon^2 t \cdots .$$

Accordingly, differentiation with respect to time becomes

$$\frac{\mathrm{d}}{\mathrm{d}t} = \frac{\mathrm{d}T_0}{\mathrm{d}t}\frac{\partial}{\partial T_0} + \frac{\mathrm{d}T_1}{\mathrm{d}t}\frac{\partial}{\partial T_1} + \cdots = D_0 + \varepsilon D_1 + \varepsilon^2 D_2 + \cdots,$$

$$\frac{\mathrm{d}^2}{\mathrm{d}t^2} = D_0^2 + 2\varepsilon D_0 D_1 + \varepsilon^2(D_1^2 + 2D_0 D_2) + \cdots . \tag{20}$$

With the small parameter and the multiple time scales thus defined, one can proceed in the standard way [23] to construct an asymptotic approximation to the solutions of equation (18). One can easily show that the first approximation to the solution is given by

$$b(t) = \hat{b}\cos(\Omega t + \gamma) + O(\varepsilon), \tag{21}$$

where the amplitude, $\hat{b}$, and the phase, γ, satisfy the modulation equations

$$\hat{b}' = \frac{1}{\Omega}\left[-\hat{k}\sin(\gamma) + \hat{c}\Omega\frac{\hat{b}}{2}\right],$$
$$\gamma' = -\frac{\sigma}{2\Omega} + \frac{1}{\hat{b}\Omega}\left[-\hat{k}\cos(\gamma) + \frac{3}{8}\alpha_1\hat{b}^3 - \frac{1}{4}\Omega^2\alpha_2\hat{b}^3\right]. \tag{22}$$

To determine the steady state solutions, the left-hand sides of these equations are set to 0. By transforming back into the original non-dimensionalized variables, one gets the non-linear equations

$$(\hat{F}\sin\gamma)\alpha_0 + (\Omega\hat{a})c = 0,$$
$$(\hat{F}\cos\gamma)\alpha_0 - \left(\frac{3}{4}\hat{a}^3\right)\alpha_1 + \left(\frac{1}{2}\Omega^2\hat{a}^3\right)\alpha_2 + (\hat{a}\Omega^2) - (\hat{a})\omega_0^2 = 0. \tag{23}$$

Equations (23) are relatively simple and even when ω_0^2 is treated as an unknown in addition to c, α_0, α_1 and α_2, they are a linear function of the unknown parameters. The results at each excitation frequency, Ω, produce two equations of the form of equations (23). The set of linear equations generated by measuring the response at several excitation frequencies are solved in a least-squares sense to produce estimates of ω_0^2, c, α_0, α_1 and α_2.

An alternative approach, adopted here, is to eliminate γ from equations (23) and use the resulting equation in amplitude only together with the estimate of ω_0 from the free vibration transient tests. The amplitude then satisfies the non-linear equation

$$\left(\frac{9}{16}\hat{a}^6\right)\alpha_1^2 - \left(\frac{3}{4}\Omega^2\hat{a}^6\right)\alpha_1\alpha_2 + \left(\frac{1}{4}\Omega^4\hat{a}^6\right)\alpha_2^2 - \left(\frac{3}{2}(\Omega^2 - \omega_0^2)\hat{a}^4\right)\alpha_1$$
$$+ ((\Omega^2 - \omega_0^2)\Omega^2\hat{a}^4)\alpha_2 + (\hat{F}^2)\alpha_0^2 + (\Omega^2\hat{a}^2)c^2 + ((\Omega^2 - \omega_0^2)^2\hat{a}^2) = 0 \tag{24}$$

and the phase of the response is given by

$$\left(\frac{\Omega}{\tan(\gamma)}\right)c - \left(\frac{3}{4}\hat{a}^2\right)\alpha_1 + \left(\frac{1}{2}\Omega^2\hat{a}^2\right)\alpha_2 - (\Omega^2 - \omega_0^2) = 0. \tag{25}$$

The amplitude equation is more complicated and a non-linear fit to the data ($\hat{a}$ and $\hat{F}$ for each frequency Ω) is necessary to identify the unknowns (c, α_0, α_1, and α_2), even when ω_0 is assumed to be known. However, it does have the advantage that only amplitude information is required from the experiments.

As the multiple time scales theory builds its approximation around the solution at the fundamental frequency, this approach does not use higher harmonic information and, thus, is less sensitive to experimental noise. Data is extracted at the fundamental response frequency only, where the signal-to-noise ratio is very high. Limitations to this approach come with the basic assumption that the damping, non-linearity, and forcing are all of the same order, and small. The correctness of the estimated solution is dependent on this smallness. In numerical investigations where these assumptions have been violated, resulting parameter estimates have been poor.

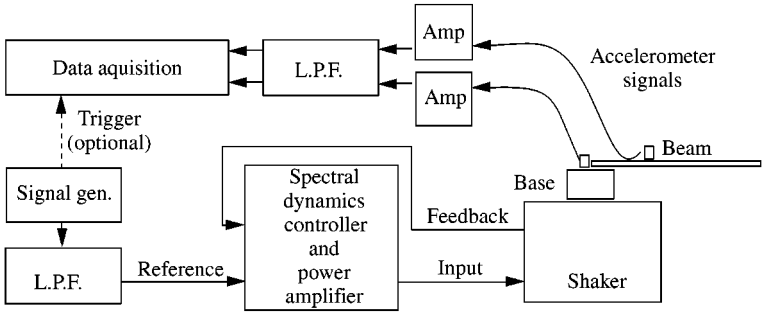

Figure 2. The experimental configuration for testing of a cantilever beam subjected to external base excitation.

3. EXPERIMENTAL INVESTIGATION: EXPERIMENTAL APPARATUS AND SAMPLE RESPONSES

Following is a description of the experimental set-up and the procedures for acquiring and processing the transient decay and steady state measurements.

3.1. EXPERIMENTAL CONFIGURATION

A schematic of the experimental configuration is given in Figure 2. The beam system was excited with a 4500 lb (2·00 kN) Thermotron electromechanical shaker. The large shaker was chosen so that the beam response at resonance would only have a small influence on the input amplitude. To further reduce this possible loading, the shaker feedback control system, a proportional gain controller, was used and the acceleration amplitude of the beam was maintained at a constant desired level.

The beams used were 0·125 in (0·318 cm) × 2·0 in (5·008 cm) 6061 T6 Aluminum bar stock cut and clamped to a length of 27 in (0·686 m). The length corresponded to a theoretical second natural frequency of 34·40 Hz, or a non-dimensional frequency (ndf) of 21·61. The mounting apparatus (base) which secures the test specimen (beam) was machined out of a single, 120 lb (54 kg), piece of 12" aluminum round-stock.

Two PCB type 353B17 2 gram accelerometers were used to measure the base and beam accelerations. The accelerometer signals were passed through PCB type 480E09 charge amplifiers with gain settings of 100 for the base-mounted accelerometer and 10 for the accelerometer secured at a distance of 7 in (0·178 m) from the clamped edge of the beam. Prior to sampling, both signals were low-pass filtered with a 24 dB/Octave roll-off Wavetek Dual Hi/Lo model 852 filter with the cut-off frequency set of 1 kHz. The Tektronix 2630 Fourier Analyzer and its Instrument Program software were used to acquire the excitation and response data. These data measurement and analysis systems have 12-bit analog-to-digital converters. Input amplitude ranges for both the excitation and response channels were set to ensure that no saturation occurred at the maximum acceleration levels.

3.2. TRANSIENT DECAY MEASUREMENT AND ANALYSIS

To simplify the parameter estimation equations in the steady state testing and to monitor any change in the beam properties during a set of tests, the transient response of the second mode of the beam was measured and analyzed to produce estimates of the undamped natural frequency (ω_0) and the damping ratio (ζ).

A low-amplitude sinusoidal excitation was generated and its frequency tuned to the beam's second undamped natural frequency (ω_0) by determining the frequency at which the input and output were 90° out of phase. Once the system had reached a steady state, the excitation was quickly removed by turning down the signal amplifier. The free vibration decay was then captured at a rate of 2560 samples/s. The anti-aliasing filter cut-off was set to 100 Hz for this test. The damping factor, ζ, was then estimated by using the log decrement technique [24]. Estimates of the natural frequency and damping ratio were in the range 33·90–34·47 Hz (ndf: 21·30–21·66) and 0·001–0·004 respectively.

The very low damping ratio meant that the beam typically took 120 s before steady state behavior was reached after changing the excitation parameters. Over the course of the steady state testing the beam was excited at high amplitudes for long periods of time, and this caused metal fatigue problems [25, 18]. Transient tests were used to ensure that the natural frequency and damping of the second mode of the beam had not changed between the start and end of the steady state tests. Changes greater than 0·029 Hz were deemed as evidence of the beam's properties having changed during the testing.

3.3. STEADY STATE TESTING

The input signals were stationary constant amplitude sine waves generated with a C program controlling an Atlanta signal processing board. The board contains a TMS320C30 chip connected to a two-channel 16-bit digital-to-analog converter (DAC). The output of the DAC was low-pass filtered to remove the high-frequency components introduced by the zero order hold digital-to-analog converter. The DAC sample rate was set to 10 kHz and the frequencies of the 35–75 excitation sinusoids used in the steady state tests were in the range of 30–35 Hz (ndf: 18·85–22·99). The analog reconstruction filter cut-off frequency was set at 100 Hz.

It was difficult to maintain a constant amplitude acceleration at the base of the beam over the range of input frequencies used because the shaker controller did not perform perfectly. Fortunately, none of the identification methods require the input amplitude to be constant over all frequencies. The methods based on harmonic balance and multiple time scales modelling require only that the input and output are at a steady state and that they are measurable.

A computer-generated external trigger signal was used to initiate the acquisition of 4096 samples (1·6 s at 2560 samples/s) of the steady state signals. This results in the acquisition of between 48 and 56 periods of the excitation, depending on the excitation frequency (30–35 Hz).

3.3.1. *Number and placement of excitation frequencies*

A detailed system identification study was carried out to provide a rationale for choosing sets of excitation frequencies in steady state tests on individual modes in structures. The study utilized data from simulations of a Duffing's equation with a hardening stiffness non-linearity. At higher amplitudes, four regions of response behavior can be identified depending on the number of possible solutions and the deviation from linear response behavior. These are shown in Figure 3.

The second mode of the cantilever beam exhibits softening behavior. However, the results of the system identification study are still pertinent because the four response regions also occur with the softening spring behavior, albeit in a different order. A brief summary of the results is given in the following paragraphs; details of the study are given in reference [26].

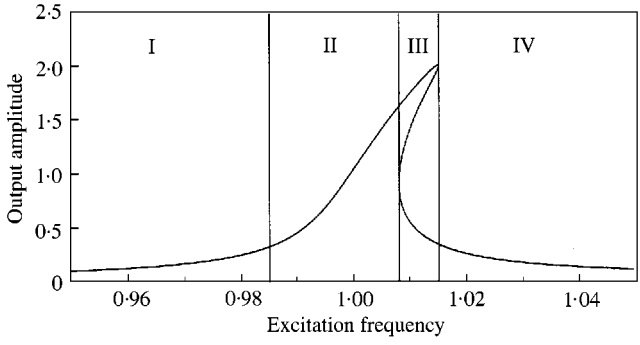

Figure 3. Illustration of regions of qualitatively different response behavior. Regions I and IV, approximately linear, region II, non-linear with one solution; region III, non-linear with two stable solutions.

Many different combinations of excitation frequencies from the four regions were utilized to determine if having more data from regions II and III would improve the accuracy of the parameter estimates. The total number of frequencies used was also varied as was the level of noise corruption. The study showed that parameter estimates tended to converge as the percentage of data from the non-linear regions (regions II and III) increased, and also as the number of frequencies used increased. At signal-to-noise ratios of 70 dB, a level typically encountered in well-controlled experiments, very little improvement in parameter estimates was observed as the percentage of data from the non-linear regions increased beyond 50%, and also as the total number of sinusoids increased above 40.

For the simulations, 832 examples of the response measurements were generated. Having set the proportion of sinusoids in each region and the total number of sinusoids, the frequencies were chosen randomly from this set of 832 finely spaced frequencies. This selection was repeated 100 times, and each time history was corrupted with a different realization of the noise time history scaled to give a prescribed signal-to-noise ratio. The mean and the standard deviation of the parameter estimates were calculated. The results from one set of simulations using harmonic balance estimation of the Duffing system parameters are plotted in Figure 4(a) against percentage of data from regions II and III. In total, 16 sinusoids were used and regions I and IV contained the same number of sinusoids. Another series of tests were conducted to track parameter estimates as a function of the number of sinusoids used; these results are shown in Figure 4(b). For these tests, the percentage in the non-linear regions was kept at 50%.

Based on these findings, the excitation frequencies used in the beam experiments were at and around the beam's natural frequency with nearly 50% of the sinusoids lying in regions II and III. In some of the experiments, the two solution region (now region II, because of the softening behavior) was very small, and hence most of the strongly non-linear data came from the adjacent region (now region III). Typically, a total of 40–60 sinusoids were used and at least half of these were in regions II and III.

3.3.2. *Measurement of input and steady state response amplitude and phase information*

The multiple time scales and harmonic balance methods incorporate amplitude and phase information, which requires the decomposition of the excitation and response into the sum of a constant plus cosines and sines of frequencies that are multiples of the excitation frequency ($k\Omega$). In both methods, as described above, the amplitude and phase information associated with the excitation frequency and certain harmonics may be used in the

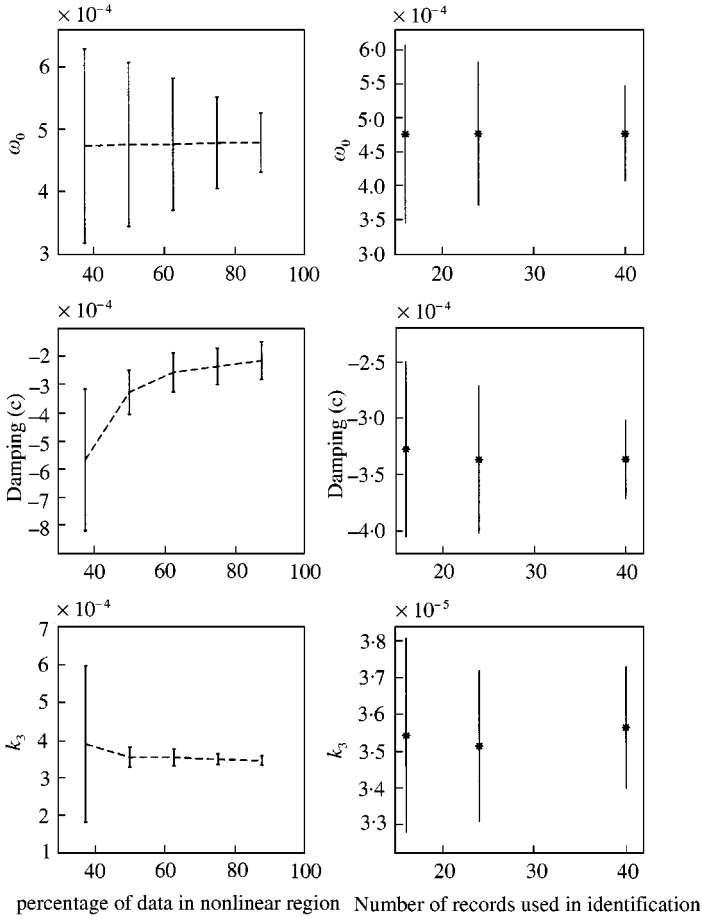

Figure 4. Harmonic balance parameter estimates for a signal-to-noise ratio of 70 dB. (Upper plots) Undamped natural frequency (ω_0), (center plots) damping coefficient (c), (lower plots) non-linear stiffness (k_3). Mean $\pm$ standard deviation as a function of (a) the percentage of data in regions II and III, and (b) the number of sinusoids used in the estimation.

parameter estimation. However, in acceleration measurements, higher harmonics, DC offsets and other noise introduced by the instrumentation will be present. Therefore, in the decomposition of the acceleration signal, the higher harmonics (up to 9Ω) and DC terms are included. The components at the frequencies of interest are extracted for use in the non-linear system identification.

Several methods can be used to estimate the amplitude and phase information of harmonic signals in the presence of noise [27]. Here, one has the added advantage of knowing the frequencies of the periodic components present in the signal because the excitation frequency (Ω) is known and the measurements are taken at steady state. The system's response is modelled as

$$a(t) = A_0 + A_{1c}\cos(\Omega t) + A_{1s}\sin(\Omega t) + A_{2c}\cos(2\Omega t) + A_{2s}\sin(2\Omega t) + A_{3c}\cos(3\Omega t)$$

$$+ A_{3s}\sin(3\Omega t) + \cdots A_{9c}\cos(9\Omega t) + A_{9s}\sin(9\Omega t) + e(t), \tag{26}$$

where $e(t)$ represents the model-data mismatch. Evaluating this equation for several different values of $t = n\Delta$, $n = 1, 2, 3, \ldots$, results in a set of linear equations, that can be written in matrix form as

$$\mathbf{A}_{cc} = \mathbf{M} \cdot \mathbf{C} + \mathbf{E}, \tag{27}$$

where $\mathbf{A}_{cc}$ is the response acceleration vector containing $a(n\Delta)$, $\mathbf{C}$ contains the harmonic amplitudes $[A_0, A_{1c}, A_{1s}, A_{2c}, A_{2s}, \ldots, A_{9c}, A_{9s}]^{\mathrm{T}}$, the matrix $\mathbf{M}$ contains rows of [1, $\cos(\Omega n\Delta)$, $\sin(\Omega n\Delta)$, $\cos(2\Omega n\Delta)$, $\sin(2\Omega n\Delta), \ldots$ $\cos(9\Omega n\Delta)$, $\sin(9\Omega n\Delta)$], and $\mathbf{E}$ contains elements $e(n\Delta)$.

$\mathbf{A}_{cc}$ and $\mathbf{M}$ are known and hence the spectral amplitudes contained in $\mathbf{C}$ can be solved for in a least-squares sense. The spectral amplitudes are found for each measurement taken at different excitation frequencies (Ω). The displacement spectral amplitudes of the components at the excitation frequency can be found analytically by integrating the terms in the model, i.e., by dividing by $-(k\Omega)^2$. The excitation's spectral amplitudes, $F_{1c}(\Omega)$ and $F_{1s}(\Omega)$, can be calculated in a similar manner. The cosine and sine spectral amplitude estimates are used directly in the harmonic balance method, while in the multiple time scales method a_{1c} and a_{1s} are squared and summed to generate the steady state amplitude $\hat{a}$ in equation (24).

3.3.3. *Integrating the response for the continuous-time method*

Digital filters can be designed to emulate integrators. The bilinear transform, often used in filter design and digital control design, is an example of a digital filter integrator that performs trapezoidal integration [28]. The sampling rate needs to be high for this filter to work well as an integrator. Digital integrators amplify low frequencies in signals which are often only present because of measurement noise. The response of the accelerometers used in the experiments falls off below 5 Hz, resulting in a low signal-to-noise ratio in this region. An alternative could be to combine a high-pass filter and an integrator, making the cut-off frequency of the high-pass filter above 5 Hz and well below the excitation frequencies used in the experiment.

However, based on the success of the signal modelling for the continuous time and the multiple time scales methods, it was decided to take a different approach to integration for these relatively simple signals. The excitation and response signals were modelled as described in the last section, and the DC component was removed. The model of the measured acceleration signal was integrated analytically once to generate the velocity signal and again to generate the displacement. The model was then used to construct the velocity and displacement time histories, and the resulting vectors were used directly in the construction of the matrix in equation (13).

Each column and the response vector is made to contain the same frequency range to compensate for the loss of high-frequency information in x, $\dot{x}$, $\ddot{x}$ due to the use of anti-aliasing filters (see section 2.2.1). Higher-frequency information is present in the columns that are non-linear functions of the displacement and velocity. If the signal model is used to calculate the non-linear functions symbolically, it is easy to remove harmonics above those that are retained in the original acceleration signal. An alternative approach, equally successful if aliasing has not occurred, is to take the displacement and velocity time histories, use them to calculate the non-linear function, fit a sum of harmonics of known frequencies model the resulting time history, remove the high-frequency components and reconstruct the signal. Both methods are effectively filtering the columns of the estimation matrix, as described in section 2.2.1, and have the advantage of avoiding the problems of

transient responses that occur when using digital filtering techniques to remove high frequencies.

4. RESULTS

The three system identification techniques described in the previous section are now applied to numerically simulated data and to measurements from experiments on the beam. The numerical data were generated by using the single-mode model given in equation (8). The parameters used in the simulation came from equations (9)–(11) (α_0, α_1, and α_2), and from the free-vibration tests described earlier (ω_0, and c). A sinusoidal force of amplitude 1 g was input to the system and time histories of the system response were generated by using a fourth order Runge–Kutta routine. The step size was fixed to be 1/64th of the period of the forcing. The integration routine introduces a time shift equal to the step size; this was subsequently removed from the numerically generated displacement and velocity data. The simulation was run until the system reached steady state, and then one period of the steady state displacement and velocity data were stored. The displacement, velocity and input history were used with the differential equation to generate the steady state acceleration data. This process was repeated for excitations at different frequencies; the frequencies used were near to the beam's second natural frequency.

Before addressing the effectiveness of each method, it must be stressed that both the harmonic balance and multiple time scales system identification techniques are based on approximate solutions to the differential equation model. As shown in Figure 5, the result of these approximations is that the predicted response amplitudes tend to deviate from the simulated response as the input amplitude increases. The harmonic balance prediction is from a single frequency expansion, later both single frequency and multiple (first and third harmonic) frequency expansions were used. In simulations, the amplitude of the input did not exceed that of the intermediate curve (1·0 g), where the amplitude predictions from all three methods were close and significant non-linearity was still observed. At higher amplitudes, a multiple time scale model that fit the steady state response data well would contain biased parameter estimates because, the illustrated in Figure 5, the true parameters would have produced a different amplitude prediction.

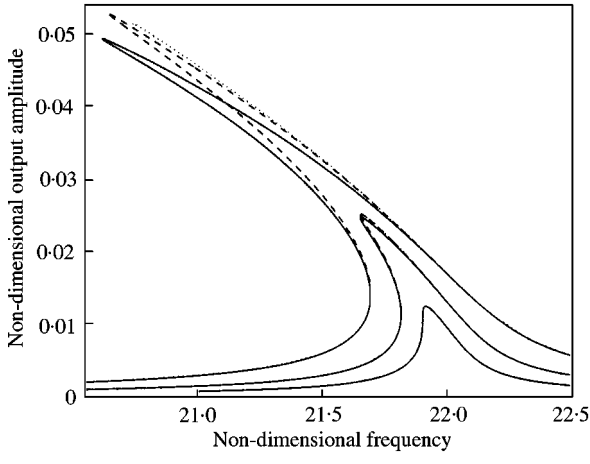

Figure 5. Response curves from simulations with three input amplitudes (0·5 g, 1·0 g, and 2·0 g): ·····, steady state response; – – – – –, predictions based on harmonic balance; ——, predictions based on multiple time scales. Assumed system parameters are: $\omega_0 = 2{\cdot}20 \times 10^1$, $c = 1{\cdot}16 \times 10^{-2}$, $\alpha_0 = 4{\cdot}34 \times 10^{-1}$, $\alpha_1 = 1{\cdot}34 \times 10^4$, $\alpha_2 = 1{\cdot}44 \times 10^2$.

Keeping this in mind, system identification was performed on numerical and experimental data. The natural frequency (ω_0) was assumed to be known from the free vibration tests, and the remaining parameters, including damping, were estimated by using each of the three methods. Two variations of the methods were also investigated because of the results from various simulations and experiments. First, the multiple time scales approach was extended to incorporate the phase information and the parameters were estimated from sets of equations based on equations (23). Secondly, in the experimental data analysis the equations for the harmonic balance method with only one harmonic term were also used for parameter estimation. The results of these two methods, when used, are shown

TABLE 1

Coefficient estimates with simulation data for high amplitude excitation (1·0*g*)

Parameter	Actual value	Continuous time	Harmonic balance	Multiple time scales (with phase)
ω_0 (fixed)	$2{\cdot}20 \times 10^{1}$	$2{\cdot}20 \times 10^{1}$	$2{\cdot}20 \times 10^{1}$	$2{\cdot}20 \times 10^{1}$ ($2{\cdot}20 \times 10^{1}$)
c	$4{\cdot}42 \times 10^{-2}$	$4{\cdot}43 \times 10^{-2}$	$4{\cdot}43 \times 10^{-2}$	$5{\cdot}24 \times 10^{-2}$ ($4{\cdot}14 \times 10^{-2}$)
α_0	$4{\cdot}34 \times 10^{-1}$	$4{\cdot}36 \times 10^{-1}$	$4{\cdot}36 \times 10^{-1}$	$4{\cdot}34 \times 10^{-1}$ ($4{\cdot}33 \times 10^{-1}$)
α_1	$1{\cdot}34 \times 10^{4}$	$1{\cdot}39 \times 10^{4}$	$1{\cdot}39 \times 10^{4}$	$2{\cdot}92 \times 10^{4}$ ($2{\cdot}83 \times 10^{4}$)
α_2	$1{\cdot}44 \times 10^{2}$	$1{\cdot}46 \times 10^{2}$	$1{\cdot}46 \times 10^{2}$	$1{\cdot}92 \times 10^{2}$ ($1{\cdot}90 \times 10^{2}$)
$\hat{\alpha}_1$	$1{\cdot}00 \times 10^{5}$	$9{\cdot}97 \times 10^{4}$	$9{\cdot}97 \times 10^{4}$	$9{\cdot}88 \times 10^{4}$ ($9{\cdot}87 \times 10^{4}$)

TABLE 2

Coefficient estimates from experimental data at low amplitude excitation (1·0*g*)

Parameter	Continuous time	Harmonic balance (first harmonic only)	Multiple time scales (with phase)
ω_0 (fixed)	$2{\cdot}17 \times 10^{1}$	$2{\cdot}17 \times 10^{1}$ ($2{\cdot}17 \times 10^{1}$)	$2{\cdot}17 \times 10^{1}$ ($2{\cdot}17 \times 10^{1}$)
c	$1{\cdot}21 \times 10^{-1}$	$1{\cdot}21 \times 10^{-1}$ ($1{\cdot}20 \times 10^{-1}$)	$1{\cdot}54 \times 10^{-1}$ ($1{\cdot}20 \times 10^{-1}$)
α_0	$4{\cdot}38 \times 10^{-1}$	$4{\cdot}38 \times 10^{-1}$ ($4{\cdot}36 \times 10^{-1}$)	$4{\cdot}44 \times 10^{-1}$ (4.36×10^{-1})
α_1	$-6{\cdot}00 \times 10^{4}$	$-5{\cdot}98 \times 10^{4}$ ($-12{\cdot}8 \times 10^{4}$)	$-83{\cdot}0 \times 10^{4}$ ($-12{\cdot}8 \times 10^{4}$)
α_2	$-9{\cdot}98 \times 10^{1}$	$-9{\cdot}93 \times 10^{1}$ ($-32{\cdot}7 \times 10^{1}$)	$-267{\cdot}0 \times 10^{1}$ ($-32{\cdot}7 \times 10^{1}$)
$\hat{\alpha}_1$	$8{\cdot}94 \times 10^{4}$	$8{\cdot}91 \times 10^{4}$ ($8{\cdot}71 \times 10^{4}$)	$6{\cdot}55 \times 10^{4}$ ($8{\cdot}71 \times 10^{4}$)

TABLE 3

Coefficient estimates with simulation data at low amplitude excitation (0·5*g*)

Parameter	Actual value	Continuous time	Harmonic balance	Multiple time scales (with phase)
ω_0 (fixed)	$2{\cdot}20 \times 10^{1}$	$2{\cdot}20 \times 10^{1}$	$2{\cdot}20 \times 10^{1}$	$2{\cdot}20 \times 10^{1}$ ($2{\cdot}20 \times 10^{1}$)
c	$1{\cdot}16 \times 10^{-1}$	$1{\cdot}16 \times 10^{-1}$	$1{\cdot}16 \times 10^{-1}$	$1{\cdot}16 \times 10^{-1}$ ($1{\cdot}16 \times 10^{-1}$)
α_0	$4{\cdot}34 \times 10^{-1}$	$4{\cdot}34 \times 10^{-1}$	$4{\cdot}34 \times 10^{-1}$	$4{\cdot}33 \times 10^{-1}$ ($4{\cdot}34 \times 10^{-1}$)
α_1	$1{\cdot}34 \times 10^{4}$	$1{\cdot}14 \times 10^{4}$	$1{\cdot}14 \times 10^{4}$	$1{\cdot}04 \times 10^{4}$ ($1{\cdot}27 \times 10^{4}$)
α_2	$1{\cdot}45 \times 10^{2}$	$1{\cdot}38 \times 10^{2}$	$1{\cdot}38 \times 10^{2}$	$1{\cdot}35 \times 10^{2}$ ($1{\cdot}42 \times 10^{2}$)
$\hat{\alpha}_1$	$10{\cdot}0 \times 10^{4}$	$9{\cdot}97 \times 10^{4}$	$9{\cdot}97 \times 10^{4}$	$9{\cdot}95 \times 10^{4}$ ($9{\cdot}94 \times 10^{4}$)

TABLE 4

Coefficient estimates from experimental data at high amplitude excitation (1·5*g*)

Parameter	Continuous time	Harmonic balance (first harmonic only)	Multiple time scales (with phase)
ω_0 (fixed)	$2{\cdot}17 \times 10^{1}$	$2{\cdot}17 \times 10^{1}$ ($2{\cdot}17 \times 10^{1}$)	$2{\cdot}17 \times 10^{1}$ ($2{\cdot}17 \times 10^{1}$)
c	$1{\cdot}74 \times 10^{-1}$	$1{\cdot}74 \times 10^{-1}$ ($1{\cdot}75 \times 10^{-1}$)	$1{\cdot}95 \times 10^{-1}$ ($1{\cdot}75 \times 10^{-1}$)
α_0	$4{\cdot}34 \times 10^{-1}$	$4{\cdot}34 \times 10^{-1}$ ($4{\cdot}38 \times 10^{-1}$)	$4{\cdot}57 \times 10^{-1}$ (4.38×10^{-1})
α_1	$-7{\cdot}83 \times 10^{4}$	$-7{\cdot}82 \times 10^{4}$ ($1{\cdot}82 \times 10^{4}$)	$-7{\cdot}35 \times 10^{4}$ ($1{\cdot}83 \times 10^{4}$)
α_2	$-1{\cdot}68 \times 10^{2}$	$-1{\cdot}68 \times 10^{2}$ ($1{\cdot}57 \times 10^{2}$)	$-1{\cdot}53 \times 10^{2}$ ($1{\cdot}57 \times 10^{2}$)
$\hat{\alpha}_1$	$8{\cdot}22 \times 10^{4}$	$8{\cdot}21 \times 10^{4}$ ($8{\cdot}83 \times 10^{4}$)	$8{\cdot}15 \times 10^{4}$ ($8{\cdot}83 \times 10^{4}$)

in parentheses in Tables 1–4. In addition to the coefficients of the non-linear terms, α_1, α_2, a combination of these two terms, $\hat{\alpha}_1$, is also given, where $\hat{\alpha}_1 = -3\alpha_1 + 2\omega_0^2\alpha_2$. This term appears when slightly different detuning is used when deriving the multiple time scales equations, and in that case α_1 and α_2 do not appear other than in this combined form.

The parameter estimates were used to generate amplitude and phase response predictions in order that they may be compared to the simulated or measured response amplitudes and phases. The harmonic balance amplitude and phase equations were used with both the continuous time and the harmonic balance parameter estimates to predict the system's

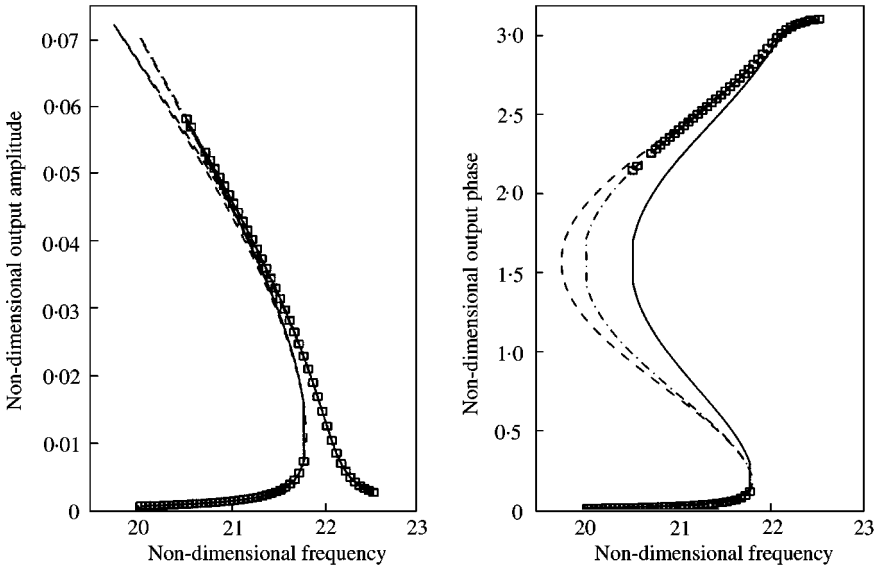

Figure 6. Response curves with simulation data for high amplitude excitation (1·0 *g*). □, steady state response; ·····, predictions based on continuous time estimates; – – – – –, predictions based on harmonic balance estimates; ——, predictions based on amplitude only multiple time scales estimates; – · – – · –, predictions based on amplitude and phase multiple time scales estimates.

response. The multiple time scales estimates were used in the multiple time scales amplitude and phase equations.

4.1. FIRST SIMULATION

Amplitude and phase shifts for the numerically generated displacement responses are shown in Figure 6 as a function of the excitation frequency. The response predictions using the parameters estimated from different techniques are also shown in this figure, and the parameter estimates are given in Table 1.

Most of the parameters are estimated well. The exceptions are the estimates of α_1 and α_2 resulting from the multiple time scales methods. The multiple time scales estimates of the combined term, $\hat{\alpha}_1$, however, are reasonably accurate. Most of the response predictions are good with the exception of the phase prediction using the multiple time scales without phase information, and the amplitude prediction at high response levels using the multiple time scales with phase information.

4.2. FIRST EXPERIMENT

The simulation results indicated that an accurate estimation of the system parameters was possible. Therefore, input and output data were collected from the experimental system forced at the same level of excitation (1 *g*), and the identification steps were repeated. The experimental response data along with the predicted responses using the estimated parameters from the three identification techniques are shown in Figure 7. The parameter estimates are shown in Table 2.

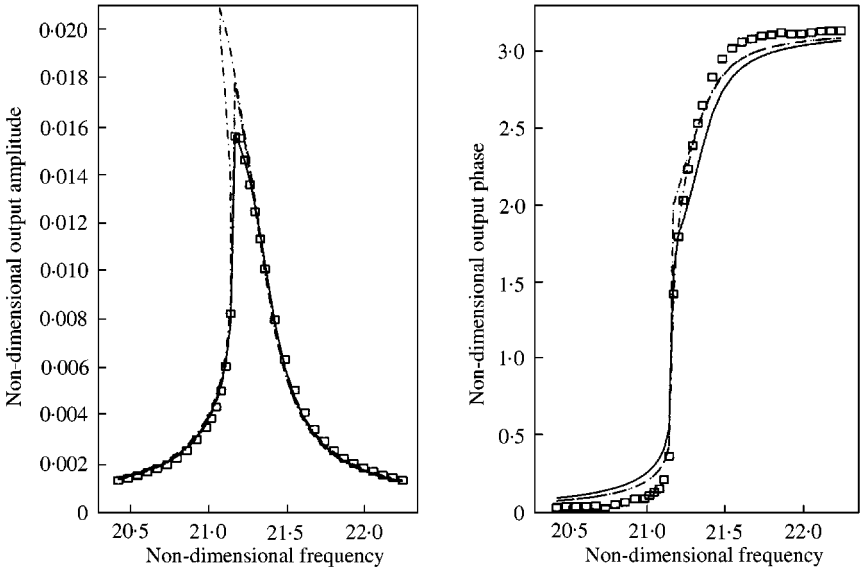

Figure 7. Response curves with experimental data at low amplitude excitation (1·0 g). □, steady state response; ·····, predictions based on continuous time estimates; – – – – – predictions based on harmonic balance estimates; ——, predictions based on amplitude only multiple time scales estimates; – · – – · –, predictions based on amplitude and phase-multiple time scales estimates.

Unlike in the simulation, the two solution region is either very small or not present in the experimental data. This can partially be explained by the system's damping which was estimated here to be nearly 3 times its value in the simulations. All methods produced similar estimates for the damping coefficient and the coefficient of the forcing term. Each method produced negative values for α_1 and α_2, which is not consistent with their theoretical definitions as given in equations (9) and (10). The combined term parameter, $\hat{\alpha}_1$, was much closer to its theoretical value. The harmonic balance method based on a one-term expansion gave estimates very close to those produced by the multiple time scales method that uses phase information. Since these methods essentially use the same information, perhaps this is not surprising.

As shown in Figure 7, the system's overall response was well predicted irrespective of which set of estimated parameters were used, even though there were sometimes large differences between the parameter estimates. The inclusion of phase information in the multiple time scales estimation resulted in a better prediction of the phase response, although with these parameters the model predicted larger response amplitudes than were measured. The multiple time scales without phase estimates resulted in accurate predictions of the response amplitudes.

Intuitively, non-linear parameter estimation is likely to be most successful when the data used in the estimation is collected while the system is behaving nonlinearly. To determine whether the poorer estimates were the result of data that were weakly influenced by the system non-linearity, two more tests, a simulation and an experiment, were conducted.

4.3. SECOND SIMULATION

First, in order to investigate if the poor estimates were due to the lack of a large *non-linear response region*, numerical data sets were generated which did not demonstrate the jump

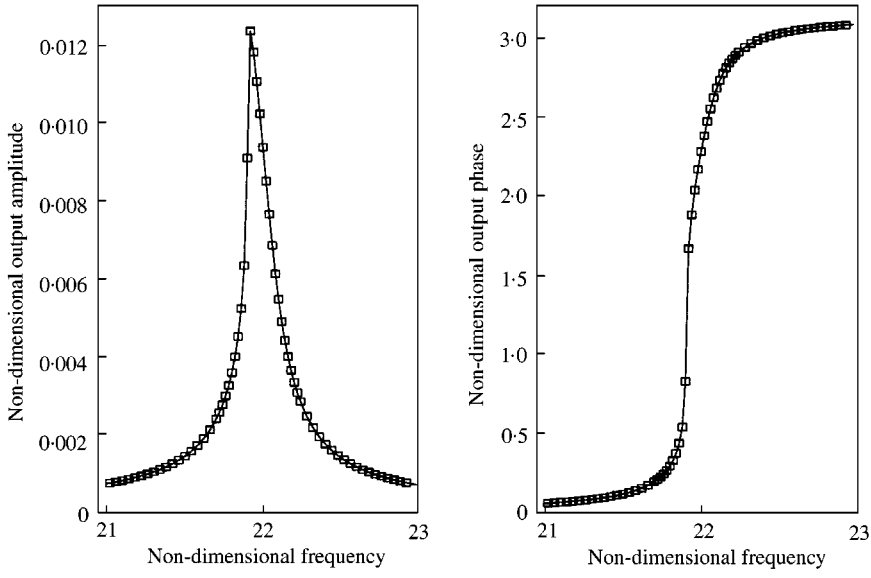

Figure 8. Response curves with simulation data at low amplitude excitation (0·5 *g*). □, steady state response; ·····, predictions based on continuous time estimates; – – – – –, predictions based on harmonic balance estimates; ——, predictions based on amplitude only multiple time scales estimates; – · – · – ·, predictions based on amplitude and phase multiple time scales estimates.

phenomenon. A lower input amplitude (0·5 g) and a higher damping coefficient ($c = 0{\cdot}116$) were used. The response predictions are shown in Figure 8, and the parameter estimates are given in Table 3.

The parameter estimates and the response predictions arising from them are accurate, even though the non-linear region is small. The addition of experimental noise combined with a very small or non-existent two solution region still did not lead to negative non-linear coefficients. This was true for signal-to-noise ratios as low as 30 dB, far lower than that encountered in the experiment.

4.4. SECOND EXPERIMENT

Next an experiment was conducted with a larger input amplitude assuring a clear jump in the beam's steady state response data. The two solution region was still very small. Experiments conducted at higher amplitudes of excitation resulted in cracks forming in the beam during the period of the steady state testing and sometimes the beam broke in two. 1·5 g was the highest level of excitation that could be used without initiating cracks during the experiments. The response predictions from the estimated models are shown in Figure 9, and the parameter estimates as given in Table 4.

All methods perform well in terms of response prediction; the greatest discrepancies were observed in the phase predictions. Too high a damping coefficient estimate would result in the differences between the predictions and measurements of the phase of the response. However, lowering the damping would result in an increase in the response amplitude predictions which are currently very accurate.

Again, the problem of negative values for the estimates of α_1 and α_2 arose. However, when the phase was included in the multiple time scales estimation, or when the one-term

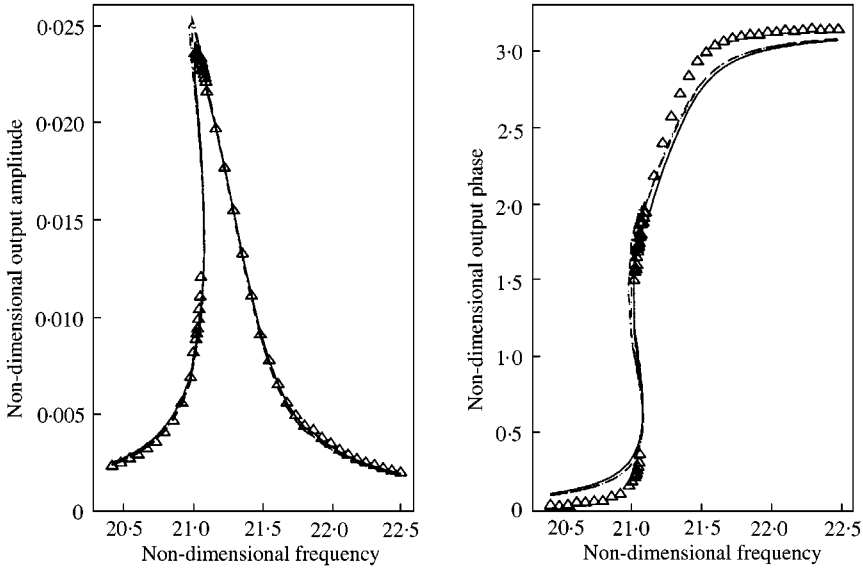

Figure 9. Response curves with experimental data at high amplitude excitation (1·5 g). △, steady state response; ·····, predictions based on continuous time estimates; – – – – –, predictions based on harmonic balance estimates; ——, predictions based on amplitude only multiple time scales estimates; – · – – · –, predictions based on amplitude and phase multiple time scales estimates.

harmonic balance solution was used in the estimation, the resulting coefficient estimates were positive and were reasonably close to the theoretical values that were used in simulations.

4.5. EXPERIMENTAL MODEL PREDICTION CAPABILITIES

It is a concern in system identification that models may only predict the data used for parameter estimation and the true system behavior is not captured. In order to test the estimated models' predictive capabilities, the parameter estimates resulting from the lower amplitude excitation of the beam were used to predict the response of the beam at a higher level of excitation, and *vice versa*. For this comparison, only the estimates from the multiple time scales method that uses both amplitude and phase information were utilized. Similar results were achieved by using the estimates from the other methods. As before, the multiple time scales modulation equations were used to predict the response amplitudes and phases. The results are shown in Figure 10.

The amplitude predictions at lower response levels, i.e., away from resonance, are close to the measured responses for both models. However, at the higher response amplitudes, near resonance, the model based on estimates from high-level excitation data predicts response amplitudes that are lower than those measured. The model based on estimates from low amplitude excitation data predicts much higher response amplitudes than were observed at the higher excitation level. This appears to indicate a problem with the estimate, or the appropriateness of the model for damping, and perhaps a non-linear damping term may be required in the model. The phase predictions on either side of the resonance do not reach 0 and π radians, respectively, as quickly as the measured phases do, indicating that the linear damping term should be much lower than predicted. The need for non-linear damping terms has also been identified by other researchers [29].

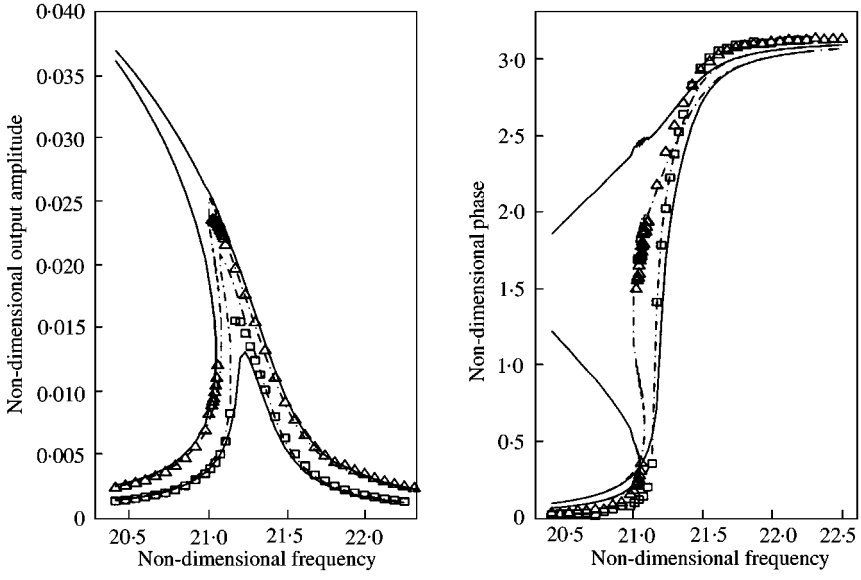

Figure 10. Comparison of predictions utilizing estimates at different excitation levels. □, low amplitude steady state response; △, high amplitude steady state response; – · – – · –, predictions based on multiple time scales estimates from data used in the estimation; ——, predictions based on multiple time scales estimates from data not used in the estimation.

5. DISCUSSION AND FURTHER ANALYSIS

In an effort to determine the sources of the differences between the theoretical and estimated models, a problem not encountered in simulations with the same levels of excitation as in the experiments, several sources of errors were investigated. First, the assumed mode shape may have been in error, and hence deviations from this would influence the α_i. Second, exclusion of the third harmonic in the harmonic balance method when applied to the experimental data led to results much closer to theory; therefore, it was speculated that at some signal-to-noise ratio the small third harmonic would be so noise corrupted that including it would be detrimental to the parameter estimation process. Third, the differences in the damping estimates between the low and high amplitude excitation indicated that it may be appropriate to include a non-linear damping term. Fourth, the error surface as a function of the two non-linear term coefficients, α_1 and α_2, was generated to determine the sensitivity of the least-squares estimation to error.

5.1. INFLUENCE OF MODE SHAPE VARIATIONS

In the theoretical development a linear mode shape was used to determine the theoretical coefficients α_1 and α_2, which may introduce significant errors because these non-linear term coefficients are complicated functions of the mode shape, as shown in equations (9)–(10).

The accelerometer used to measure the beam acceleration in the experiment can be modelled as a point mass added to the beam. When the point mass is accounted for in the modal function $\phi(s)$, a new linear mode shape is determined. (This development parallels the work done in reference [18].) The resulting linear mode is shown with the original linear mode, both non-dimensionalized, in Figure 11(a). The two modes are very close, and despite

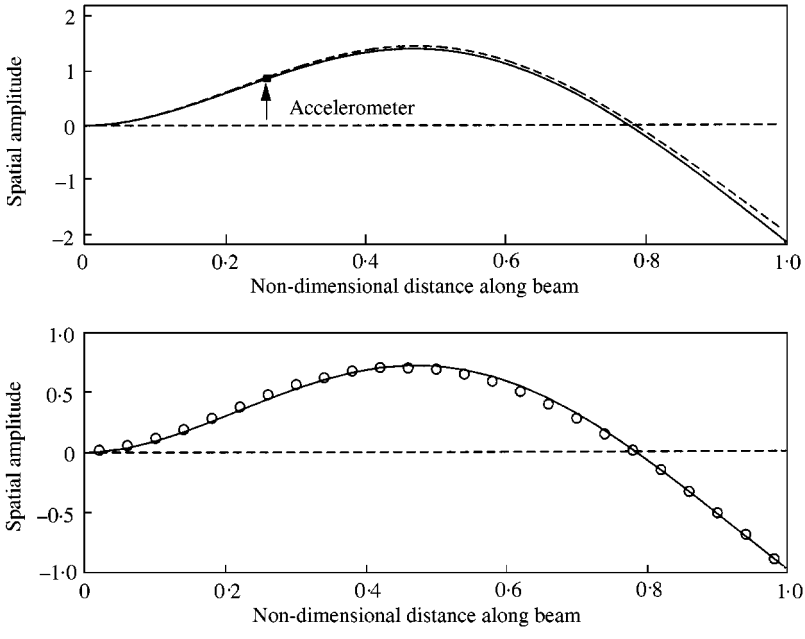

Figure 11. Variations in mode shape: (a) ——, linear non-dimensionalized mode shape; – – modified linear non-dimensionalized mode shape; (b) ——, linear mode shape; ◦, measured mode shape.

the complexity of the α_i equations, the resulting changes in the theoretical α_1 and α_2 were insignificant: the new mode shape shifted α_1 from $1{\cdot}34 \times 10^4$, $1{\cdot}32 \times 10^4$ and α_2 from $1{\cdot}45 \times 10^2$ to $1{\cdot}44 \times 10^2$.

The clamping of the beam is also imperfect and thus the boundary conditions used in generating the mode shape are not strictly correct. This effect is sometimes approximated by assuming that the beam is of a different length, but still with the perfect clamping. This does not change the shape and thus would not result in a change in the non-linear term coefficients. However, the length that would correspond to the measured second natural frequency with perfect clamping would be 0·6899 m, 4·1 mm longer than the actual length from the clamp to the free end. The experimentally measured mode shape, shown in Figure 11(b), was very close to the theoretical mode shape indicating that the natural frequency discrepancies could perhaps be more properly attributed to material property variations.

5.2. INFLUENCE OF NOISE CORRUPTION ON THIRD HARMONIC

Another possible explanation for the discrepancy between the theoretical and experimentally estimated α_i is noise corruption. The influence of noise on the parameter estimation was investigated as even small amounts of noise, like those present in the experiment, can have a pronounced effect on the relatively small amplitudes at the third harmonic.

A one-term harmonic balance based identification was implemented on the experimental data in appreciation of the noise-sensitive third-harmonic information. The results (section 4) indicate that the estimates of α_1 and α_2 were much closer to theoretical values when the third harmonic was not used. This information alone does not prove that experimental

TABLE 5

Coefficient estimates with simulation data: high amplitude excitation (1·0*g*)

Parameter	Harmonic balance (noise-free)	Harmonic balance (10 dB)	Harmonic balance (60 dB)	Harmonic balance (80 dB)
ω_0 (fixed)	$2{\cdot}20 \times 10^{1}$	$2{\cdot}20 \times 10^{1}$	$2{\cdot}20 \times 10^{1}$	$2{\cdot}20 \times 10^{1}$
c	$4{\cdot}43 \times 10^{-2}$	$4{\cdot}30 \times 10^{-2}$	$4{\cdot}43 \times 10^{-2}$	$4{\cdot}43 \times 10^{-2}$
α_0	$4{\cdot}36 \times 10^{-1}$	$4{\cdot}20 \times 10^{-1}$	$4{\cdot}36 \times 10^{-1}$	$4{\cdot}36 \times 10^{-1}$
α_1	$1{\cdot}39 \times 10^{4}$	$1{\cdot}33 \times 10^{4}$	$1{\cdot}39 \times 10^{4}$	$1{\cdot}39 \times 10^{4}$
α_2	$1{\cdot}46 \times 10^{2}$	$1{\cdot}44 \times 10^{2}$	$1{\cdot}46 \times 10^{2}$	$1{\cdot}46 \times 10^{2}$
$\hat{\alpha}_1$	$9{\cdot}97 \times 10^{5}$	$9{\cdot}89 \times 10^{4}$	$9{\cdot}97 \times 10^{4}$	$9{\cdot}97 \times 10^{4}$

noise was detrimental to the identification, and while it is safe to assume that the third harmonic suffers significantly from the experimental noise, other factors may be involved such as other modes contributing to the measured response. Recall that with the relatively noise-free simulation data, inclusion of the third harmonic was shown to help the identification.

To investigate the direct effects of noise on the parameter estimation, noise was added to the simulation data, generating overall signal-to-noise ratios (SNR) ranging from 10 to 80 dB. This corresponded to a signal-to-noise ratio at the third harmonic between -10 and 60 dB. Harmonics estimated from the corrupted data were then used in identifying the system parameters. Ten runs were performed at each noise level and the results which varied most from the noise-free estimates are reported in Table 5.

The results show that while the noise does affect the estimation, the level of noise in the experiment (around 60 dB SNR) does not account for the large variations between theory and the values obtained with the experimental data.

5.3. INFLUENCE OF NON-LINEAR DAMPING

A mismatch between model and physical system may also contribute to discrepancies between the theory and the experimental parameters. Deviations in the predicted and measured phases from the experimental tests indicate that the linear damping term may not be sufficient. A quadratic damping term has been used in modelling similar systems [29]. The effects of including this term are presented here.

While increasing the linear damping had the effect of improving the fit to the measured phase in the region very close to resonance, the fit away from resonance deteriorated. The behavior away from resonance indicates the presence of a very low level of linear damping. The inclusion of a term in the model of the form

$$d\dot{b}|\dot{b}|^{\gamma}, \tag{28}$$

where d and γ are constants, would have the effect of significantly increasing the damping present at high amplitudes of response while having a much smaller influence at low levels of response. A particular value of γ was chosen *a priori* by first assuming that the estimate of $c = 2\zeta\omega_0$, the linear portion of the damping term, was correct in the small amplitude transient tests. Then it was also assumed that the increase in damping in the low and high amplitude steady state tests produced a reasonable estimate of the total damping force at those amplitudes of response. From these assumptions, the following equations are

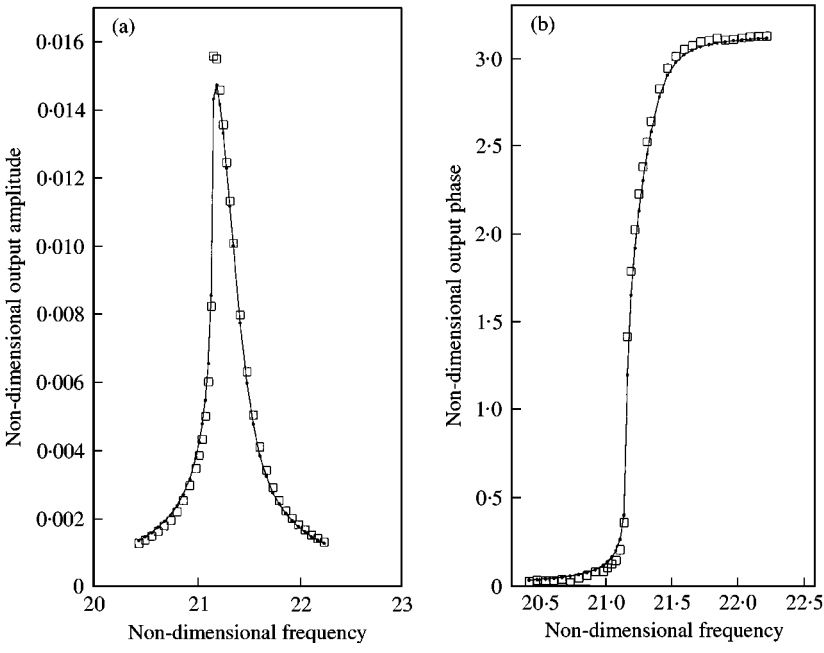

Figure 12. Response curves using a non-linear damping term with experimental data: low amplitude excitation. Steady state response (□), and predictions based on continuous time method (——). The model parameters are; $\omega_0 = 2{\cdot}13 \times 10^1$, $c = 4{\cdot}42 \times 10^{-2}$, $d = 4{\cdot}44 \times 10^{-1}$, $\alpha_0 = 4{\cdot}50 \times 10^{-1}$, $\alpha_1 = -6{\cdot}03 \times 10^4$, $\alpha_2 = -9{\cdot}99 \times 10^1$.

derived:

$$d\dot{b}_{high}|\dot{b}_{high}|^{\gamma} = (c_{ss-high} - c_{transient})\dot{b}_{high} \tag{29}$$

and

$$d\dot{b}_{low}|\dot{b}_{low}|^{\gamma} = (c_{ss-low} - c_{transient})\dot{b}_{low}, \tag{30}$$

where $\dot{b}_{low}$ and $\dot{b}_{high}$ are determined from the steady state response data in the non-linear region where the fit of the models is very good. An estimate of γ can be found by simultaneously solving equations (29) and (30). The range of possible values for γ determined by using this approximation and various experimental results is from 0·957 to 1·54. The inclusion of this term in the model with γ set to one and re-estimating the coefficients, while fixing the linear damping term to its estimated value from the low amplitude transient tests, produced the parameters and corresponding predicted curves shown in Figures 12 and 13.

It is demonstrated that the inclusion of the non-linear damping term enhances the nearness of the predicted curves to the measured data. Still, the new model form does not bring the estimated α_1 and α_2 any closer to their theoretical predictions, and in this regard the study does nothing to explain the difference.

5.4. ERROR SURFACE AS A FUNCTION OF α_1 AND α_2

Finally, the error surface was generated in an attempt to understand the significance of this difference between the theoretical and experimentally determined α_1 and α_2. Clearly,

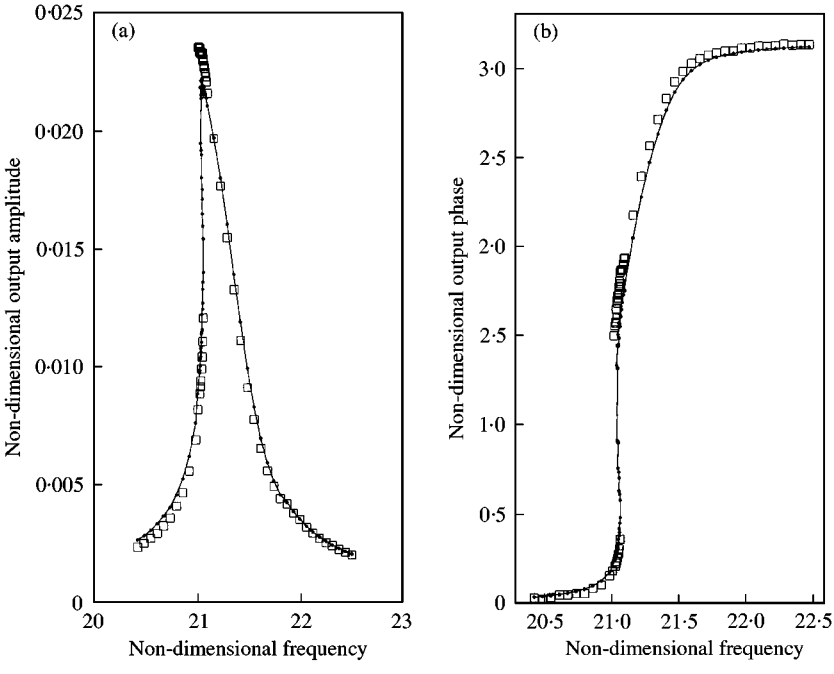

Figure 13. Response curves using a non-linear damping term with experimental data: high amplitude excitation. Steady state response (□), and predictions based on continuous time method (——). The model parameters are: $\omega_0 = 2{\cdot}13 \times 10^1$, $c = 4{\cdot}42 \times 10^{-2}$, $d = 4{\cdot}46 \times 10^{-1}$, $\alpha_0 = 4{\cdot}75 \times 10^{-1}$, $\alpha_1 = -7{\cdot}85 \times 10^4$, $\alpha_2 = -1{\cdot}68 \times 10^2$.

the individual terms are quite different. It is also apparent that the combined non-linear effect (which can be loosely thought of as the $\hat{\alpha}_1$ term, described in section 4) is approximately the same. An appreciation of this nearness can be seen when the error is examined as a function of α_1 and α_2.

To generate the error surface, the multiple time scales-based system identification method was modified. The values for α_1 and α_2 were varied while all the others were fixed to those known or determined from the estimation. Then, for each (α_1, α_2) pair the total error was calculated and plotted, as shown in Figure 14. Included in the plot is the (α_1, α_2) point associated with the minimum found by the non-linear solver and the theoretical (α_1, α_2) point.

The two solution sets lie in a trough along a line of constant $\hat{\alpha}_1$, and thus when even low level of experimental noise are introduced, the algorithm will have difficulty in locating the true minimum in this trough region. Use of the noise-free simulation data (Figure 14(b)) is shown to define the solution space more precisely. Adding noise to the simulation data raised the error surface and introduced slight lateral translations and rotations to the trough.

6. SUMMARY AND CONCLUSIONS

Three methods for system identification of a one-mode non-linear model of a base excited beam undergoing transverse vibrations were studied: continuous-time estimation, harmonic balance estimation, and multiple time scales estimation. The responses in small amplitude transient tests and higher amplitude sinusoidal tests at steady state were used to

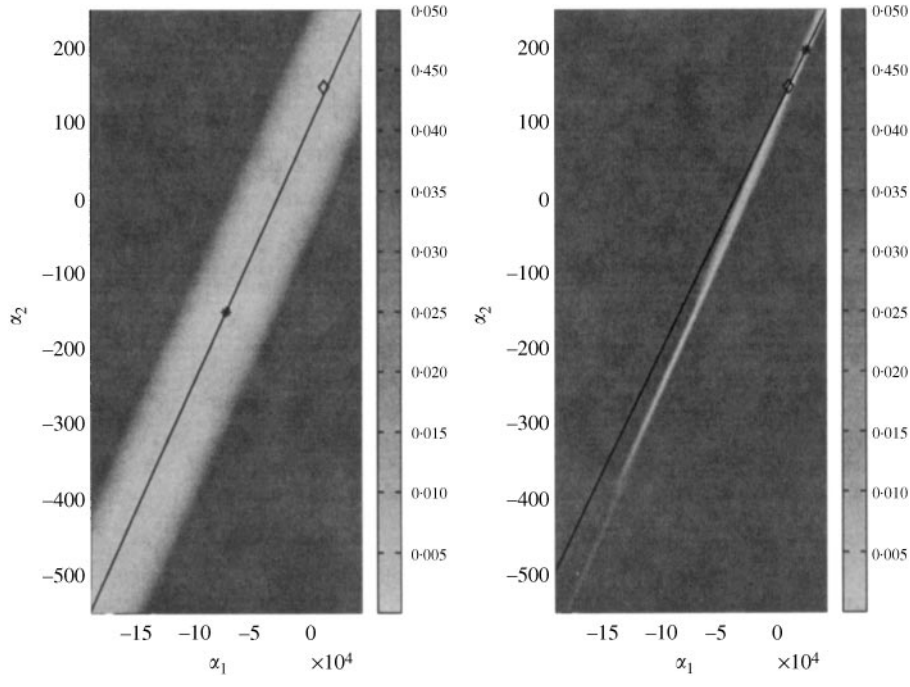

Figure 14. Error in the multiple time scales estimation as a function of α_1 and α_2: (a) experimental data ($\omega_0 = 2{\cdot}13 \times 10^1$, $c = 1{\cdot}95 \times 10^{-2}$, $\alpha_0 = 4{\cdot}57 \times 10^{-1}$), and (b) simulation data ($\omega_0 = 2{\cdot}20 \times 10^1$, $c = 1{\cdot}16 \times 10^{-2}$, $\alpha_0 = 4{\cdot}34 \times 10^{-1}$). $*$, minimum value; $\diamond$, theoretical estimates; ——, line corresponding to $\hat{\alpha}_1 =$ constant.

determine model parameters. Both simulated and experimental data were used to determine or eliminate the possible causes of theory–experiment mismatch.

While in simulation data it was found to be advantageous to include higher harmonic information, in experimental data this led to larger mismatches with theoretical predictions. This could have been the result of errors in the measurement and predictions of contributions of the higher harmonics caused by noise and filtering introduced to avoid aliasing. In simulations at high signal-to-noise ratios the continuous-time method, a direct use of the differential equation modelling the modal behavior, produced the best parameter estimates. In experiments, the parameter estimates closest to theory were produced by using a one-term harmonic balance model of the response, or by using the multiple time scales method utilizing both amplitude and phase information.

Even when estimates of the coefficients of the non-linear terms were far from their theoretical values, they still produced good predictions of the response amplitude and phase behavior. The error surface as a function of the non-linear coefficients had a *trough-like* appearance, and the error slowly decreased towards the minimum along the floor of this trough. With this type of error surface, noise has the effect of producing large variability in the estimates in the direction of the trough floor. The poor estimates of the coefficients of the non-linear terms may have resulted from this problem.

Analysis of models generated from tests with different levels of excitation indicated a problem with the linear damping model. Low amplitude tests produced much lower damping coefficient estimates than high amplitude tests. Introduction of an additional non-linear damping term led to improvements in the model, but good models were only estimated when the linear damping term was fixed at the value determined in the low-level transient tests.

ACKNOWLEDGMENTS

This work was supported, in part, by the National Science Foundation through the grant CMS-9402278. Dr Devendra Garg was the project monitor.

REFERENCES

1. L. LJUNG 1987 *System Identification*: *Theory for the User*. Englewood Cliffs, NJ: Prentice-Hall. Inc.
2. T. SODERSTROM and P. STOICA 1988 *System Identification*. Englewood Cliffs, NJ: Prentice-Hall, Inc.
3. S. A. BILLINGS 1980 *Proceedings of IEEE* **127**(**D**), 272–285. Identification of nonlinear systems—a survey.
4. P. DAVIES 1993 *Proceedings of Vibration Engineering Seminar*, *Taejon*, *Korea*, 101–116. Nonlinear system modeling and identification.
5. P. YOUNG 1996 *Proceedings of the International Conference on Identification in Engineering Systems*, *Swansea*, 1–17. Identification, estimation and control of continuous-time and delta operator systems.
6. R. HABER and H. UNBEHAUEN 1990 *Automatica* **26**, 651–677. Structure identification of nonlinear dynamic systems-a survey on input/output approaches.
7. S. CHEN and S. A. BILLINGS 1989 *International Journal of Control* **49**, 1013–1032. Representations of non-linear systems: the NARMAX model.
8. S. A. MCCABE 1998 *Ph.D. Thesis*, *Purdue University*. Nonlinear digital system identification of vibrating structures.
9. D. J. MOOK 1989 *American Institute of Aeronautics and Astronautics Journal* **27**, 968–974. Estimation and identification of nonlinear dynamic systems.
10. T. KAVZOGLU and P. M. MATHER 1999 *International Journal of Remote Sensing* **20**, 2787–2803. Pruning artificial neural networks: an example using land cover classification of multi-sensor images.
11. J. A. GOTTWALD, L. N. VIRGIN and E. H. DOWELL 1992 *Journal of Sound and Vibration* **158**, 447–467. Experimental mimicry of duffing's equation.
12. M. D. TODD, L. N. VIRGIN and J. A. GOTTWALD 1996 *Nonlinear Dynamics* **10**, 31–48. The nonstationary transition through resonance.
13. P. V. BAYLY and L. N. VIRGIN 1993 *Journal of Sound and Vibration* **164**, 364–374. An experimental study of an impacting pendulum.
14. K. D. MURPHY, P. V. BAYLY, L. N. VIRGIN and J. A. GOTTWALD 1994 *Journal of Sound and Vibration* **172**, 85–102. Measuring the stability of periodic attractors using perturbation-induced transients: applications to two non-linear oscillators.
15. S. L. BUX and J. W. ROBERTS 1986 *Journal of Sound and Vibration* **104**, 497–520. Non-linear vibratory interactions in systems of coupled beams.
16. R. P. ASHWORTH and A. D. S. BARR 1987 *Journal of Sound and Vibration* **118**, 47–68. The resonances of structures with quadratic inertial non-linearity under direct and parametric harmonic excitation.
17. P. F. PAI and A. H. NAYFEH 1990 *International Journal of Non-Linear Mechanics* **25**, 455–474. Non-linear non-planar oscillations of a cantilever beam under lateral base excitations.
18. L. D. ZAVODNEY and A. H. NAYFEH 1989 *International Journal of Non-linear Mechanics* **24**, 105–125. The non-linear response of a slender beam carrying a lumped mass to a principal parametric excitation: theory and experiment.
19. C. ZERETZKY and M. CRESPO DA SILVA 1994 *Journal of Sound and Vibration* **174**, 145–167. Experimental investigation of non-linear modal coupling in the response of cantilever beams.
20. M. R. M. CRESPO DA SILVA and C. C. GLYNN 1978 *International Journal of Solids and Structures* **6**, 449–461. Nonlinear flexural-flexural-torsional dynamics of inextensional beams, ii. forced motions.
21. A. L. AUDENINO and G. BELINGARDI 1996 *Mechanical Systems and Signal Processing* **10**, 277–291. Processing of simultaneous mechanical random response signals: Integration, differentiation and phase shifts correction.
22. K. YASUDA, S. KAWAMURA and K. WATANABE 1983 *Japanese Society of Mechanical Engineers International Journal* **31**, 8–14. Identification of nonlinear multi-degree-of-freedom systems (presentation of an identification technique).

23. A. H. NAYFEH and D. T. MOOK 1979 *Nonlinear Oscillations*. New York: Wiley.
24. S. S. RAO 1990 *Mechanical Vibrations*. Massachusetts: Addison-Wesley.
25. J. L. DING, J. PAZHOUH, S. B. LIN and T. D. BURTON 1994 *Scripta Metallurgica Materials* **30** 839–844. Damage characteristics by vibration test.
26. T. A. DOUGHTY, P. DAVIES, and A. K. BAJAJ 2002 On choosing inputs for nonlinear system identification. a Manuscript in preparation.
27. S. L. MARPLE JR 1987 *Digital Spectral Analysis with Applications*. Englewood Cliffs, NJ: Prentice-Hall, Inc.
28. L. R. RABINER and B. GOLD 1975 *Theory and Application of Digital Signal Processing*. Englewood Cliffs, NJ: Prentice-Hall.
29. R. W. KRAUSS and A. H. NAYFEH 1999 *Nonlinear Dynamics* **18**, 69–87. Experimental nonlinear identification of a single mode of a transversely excited beam.